Available online at www.sciencedirect.com
ScienceDirect
Journal of Solid State Chemistry 181 (2008) 1195–1203
JOURNAL OF SOLID STATE CHEMISTRY
www.elsevier.com/locate/jssc

Multivariate data analysis approach to understand magnetic properties of perovskite manganese oxides

N. Imamura[a,b], T. Mizoguchi[a], H. Yamauchi[a,b], M. Karppinen[a,b,*]

[a]*Materials and Structures Laboratory, Tokyo Institute of Technology, Yokohama 226-8503, Japan*
[b]*Laboratory of Inorganic Chemistry, Department of Chemistry, Helsinki University of Technology, FI-02015 TKK, Finland*

Received 15 January 2008; accepted 22 February 2008
Available online 29 February 2008

Abstract

Here we apply statistical multivariate data analysis techniques to obtain some insights into the complex structure-property relations in antiferromagnetic (AFM) and ferromagnetic (FM) manganese perovskite systems, $A\mathrm{MnO_3}$. The 131 samples included in the present analyses are described by 21 crystal-structure or crystal-chemical (CS/CC) parameters. *Principal component analysis* (PCA), carried out separately for the AFM and FM compounds, is used to model and evaluate the various relationships among the magnetic properties and the various CS/CC parameters. Moreover, for the AFM compounds, PLS (*partial least squares projections to latent structures*) analysis is performed so as to predict the magnitude of the Néel temperature on the bases of the CS/CC parameters. Finally, so-called PLS-DA (PLS *discriminant analysis*) method is employed to find out the most influential/characteristic CS/CC parameters that differentiate the two classes of compounds from each other.

Keywords: Multivariate data analysis; Chemometrics; Manganese perovskites; Magnetic properties; Structure-property relations

1. Introduction

In recent years, perovskite oxides have formed one of the focus areas in materials research as they exhibit a variety of physical properties that have been found exciting in both academic and technological aspects. The source of fascination is the diversity of the properties and their high sensitivity to (crystal)chemical tuning. In other words, a tiny change in chemical composition and/or crystal structure may induce huge changes in physical properties. For designing and on-demand tailoring of functional perovskite-oxide materials, it would be important to separately learn the effect of each chemical and structural parameter on the target property. These parameters are, however, often interrelated such that when examining the effect of one parameter the variations of other correlated parameters need to be taken into account. It is here that the techniques of chemometrics or statistical multivariate data analysis appear to be useful.

To approach multivariate problems various projection methods are utilized [1]. Both qualitative and quantitative investigations of correlations among the variables are possible. The so-called PCA (*principal component analysis*) method offers convenient tools for modeling and overviewing the correlation structure of a multivariate data set. It is used for searching trends, dominating variables, groups and outliers among the data. Another projection method, so-called PLS (*partial least squares projections to latent structures*) analysis, is used to look for relationships among two types of variables, i.e. x and y variables, such that the value(s) of y variable(s) may be predicted by means of x variables. Moreover, an extension of the PLS method, i.e. *discriminant analysis* (PLS-DA), provides us with a means to clarify whether the data set consists of subgroups, and how such subgroups would differ in respect to each other. Up to date the potentials provided by multivariate

*Corresponding author at. Laboratory of Inorganic Chemistry, Department of Chemistry, Helsinki University of Technology, P.O. Box 6100, FI-02015 TKK, Finland. Fax: +358 9 462 373.
E-mail addresses: maarit.karppinen@tkk.fi, karppinen@msl.titech.ac.jp (M. Karppinen).

0022-4596/$ - see front matter © 2008 Elsevier Inc. All rights reserved.
doi:10.1016/j.jssc.2008.02.025

data analysis techniques have been most intensively utilized in areas such as pharmacology, meteorology, environmental studies, economics, etc., whereas examples related to materials science problems are rare yet [2–6]. The first relevant example of the applicability of multivariate analysis methods as a tool to study crystal-structure–physical-property relations of functional perovskite-derived oxide materials concerned high-T_c superconductive copper oxides [2].

In the present study we utilize multivariate data analysis methods in examining the various relationships among the crystallographic fine structure and the magnetic properties of manganese-based perovskites, $A\mathrm{MnO_3}$. Samples selected for the study are either antiferromagnets or ferromagnets. Moreover, some of them also show—depending on the choice of the A-site cation constituent(s)—other interesting properties including the colossal magnetoresistance effect, half-metallic state, spin/charge ordering phenomenon, insulator–metal transition, etc.

2. Experimental details

2.1. Data set

The crystal-structure and magnetic-property data used in the present analysis were adopted from neutron diffraction studies published for oxygen-stoichiometric $A\mathrm{MnO_3}$ perovskites with different A-site cation compositions (as listed in Table 1). The data set consists of 131 samples (= *observations*) in total, i.e. $N_{\mathrm{TOT}} = 131$. Each sample selected for the analysis exhibits either an antiferromagnetic (AFM)–paramagnetic transition (Class-1; $N_{\mathrm{AFM}} = 76$) or a ferromagnetic (FM)–paramagnetic transition (Class-2; $N_{\mathrm{FM}} = 55$). The two compound classes were first analyzed separately. In both cases, the magnetic transition temperature, i.e. Néel temperature (T_N) for Class-1 and Curie temperature (T_C) for Class-2, was selected for the y parameter. As for the x parameters, each sample was described by altogether 21 crystal-structure or crystal-chemical (CS/CC) parameters (= *variables*), including lattice parameters and unit-cell volume, Mn–O bond lengths and Mn–O–Mn bond angles (see Fig. 1 for the definitions), average valence and average ionic radius of the A-site cation(s), *plus* other parameters that are calculated from the ionic radii, bond lengths and bond angles and believed to describe/quantify the degree of lattice distortion, the band width and the valence state of manganese. Majority of the samples included in the study are of an orthorhombically distorted perovskite structure (with four $A\mathrm{MnO_3}$ formula units *per* unit cell). However, some of the samples were originally described within a tetragonal, rhombohedral or cubic unit cell. Here all the structure data were converted *prior* to the analysis to an orthorhombic description of one perovskite unit in regards to the lattice parameters and unit-cell volume. Values for ionic radii were taken from Refs. [52,53] (at 6-coordination for Mn and 12-coordination for cation A). Detailed descriptions of the parameters utilized as x variables are given in Table 2. Here it should be noted that even though multivariate analysis can in general handle "missing data", our data tables [with $76 \times (21+1)$ inputs in the case of Class-1 and $55 \times (21+1)$ inputs in the case of Class-2] were completely filled.

2.2. Multivariate analyses

The multivariate data analyses were carried out using SIMCA-P 9.0 software (Umetrics, Sweden). For the PCA [1], the data are arranged in a matrix of N observations (76 for Class-1 and 55 for Class-2) and $21+1$ variables, and accordingly the data set can be imagined such that each observation gives a point in a 22-dimensional space. In PCA, the data are first normalized (that corresponds to giving each variable the same initial importance in the analysis) and centralized. Then the information dimensionality is reduced (on the basis of the least squares sense) by transforming the data into so-called *principal components* (PCs) that are linear combinations of the initial variables. The first PC is the line that best approximates the group of data points. The second PC must be orthogonal to the first PC and it is selected such that it improves the first approximation of the data to the maximum extent. The third PC is orthogonal to both the previous PCs and improves the approximation further, and so forth. Typically two or three PCs are enough to sufficiently model the variation in the data set. The result of the analysis is then visualized by plotting the plane defined by the first two PCs together with all the points projected onto the plane. The projection points on the plane are called *scores* (t) and the projection itself as a *score plot* ($t[1]/t[2]$). The score plot provides us with a kind of map to inspect how the observations relate to each other. To interpret the score plot further, another plot with *loading vectors* (p) is constructed as well. From the *loading plot* ($p[1]/p[2]$), it can be qualitatively read how each variable contributes to the model; accordingly it may serve as a guide for new-material engineering.

In the PLS analysis [1], the data are arranged into two matrices: the X matrix consists of the x variables (here the CS/CC parameters) and the Y matrix of the y variable(s) (here the value of T_N or T_C). In a PLS analysis in general relationships between the x and y variables are searched for such that the values of y variables may be predicted by means of x variables. Here we aim at finding the importance of each x variable on the selected y, i.e. the value of T_N or T_C. For the two matrices coordinate systems are formed, with as many dimensions as the number of variables. After the pretreatment steps, i.e. scaling and centering, PLS components that are linear combinations of the original variables are calculated like in the PCA method. The first PLS component describes the largest amount of variance, then each new one—orthogonal to the previous ones—accounts for the left-over variance maximally. From the PLS analysis, obtained is—besides the

Table 1
List of observations used in this study: 76 AFM samples (c1), 55 FM samples (c2)

Observations								
1	c1	$LaMnO_3$ [7]	45	c1	$Tb_{0.67}Ca_{0.33}MnO_3$ [26]	90	c2	$La_{0.5}Pr_{0.5}MnO_3$ [12]
2	c1	$La_{0.65}Ca_{0.35}MnO_3$ [8]	46	c1	$Tb_{0.5}Ca_{0.5}MnO_3$ [27]	91	c2	$La_{0.5}Sr_{0.5}MnO_3$ [41] (hydrothermal synthesis)
3	c1	$La_{0.4}Sr_{0.6}MnO_3$ [9]	47	c1	$Tb_{0.45}Ca_{0.55}MnO_3$ [27]			
4	c1	$La_{0.33}Ca_{0.67}MnO_3$ [10]	48	c1	$Tb_{0.4}Ca_{0.6}MnO_3$ [27]	92	c2	$La_{0.5}Sr_{0.5}MnO_3$ [9] (solid state synthesis)
5	c1	$La_{0.3}Sr_{0.7}MnO_3$ [9]	49	c1	$Tb_{0.35}Ca_{0.65}MnO_3$ [27]			
6	c1	$La_{0.25}Nd_{0.25}Ca_{0.5}MnO_3$ [11]	50	c1	$Tb_{0.33}Ca_{0.67}MnO_3$ [27]	93	c2	$La_{0.5}Sr_{0.4}Ba_{0.1}Mn_{O3}$ [42]
7	c1	$La_{0.2}Pr_{0.8}MnO_3$ [12]	51	c1	$Tb_{0.25}Ca_{0.75}MnO_3$ [27]	94	c2	$La_{0.5}Sr_{0.2}Ba_{0.3}MnO_3$ [43]
8	c1	$La_{0.2}Sr_{0.8}MnO_3$ [9]	52	c1	$Tb_{0.2}Ca_{0.8}MnO_3$ [27]	95	c2	$La_{0.5}Sr_{0.1}Ba_{0.4}MnO_3$ [43]
9	c1	$La_{0.1}Sr_{0.9}MnO_3$ [9]	53	c1	$Tb_{0.15}Ca_{0.85}MnO_3$ [27]	96	c2	$La_{0.5}Ba_{0.5}MnO_3$ [43]
10	c1	$PrMnO_3$ [13]	54	c1	$HoMnO_3$ [28]	97	c2	$La_{0.45}Sr_{0.55}MnO_3$ [9]
11	c1	$Pr_{0.975}Na_{0.025}MnO_3$ [14]	55	c1	$Ho_{0.5}Sr_{0.5}MnO_3$ [29]	98	c2	$La_{0.4}Pr_{0.6}MnO_3$ [12]
12	c1	$Pr_{0.95}Na_{0.05}MnO_3$ [14]	56	c1	$ErMnO_3$ [30]	99	c2	$La_{0.18}Pr_{0.72}Na_{0.1}MnO_3$ [44]
13	c1	$Pr_{0.95}K_{0.05}MnO_3$ [14]	57	c1	$YbMnO_3$ [31]	100	c2	$Pr_{0.925}Na_{0.075}MnO_3$ [14]
14	c1	$Pr_{0.9}Sr_{0.1}MnO_3$ [14]	58	c1	$LuMnO_3$ [32]	101	c2	$Pr_{0.9}Ca_{0.1}MnO_3$ [14]
15	c1	$Pr_{0.8}Na_{0.2}MnO_3$ [15]	59	c1	$YMnO_3$ [30]	102	c2	$Pr_{0.9}Ba_{0.1}MnO_3$ [14]
16	c1	$Pr_{0.75}Na_{0.25}MnO_3$ [16]	60	c1	$Y_{0.5}Ca_{0.5}MnO_3$ [33]	103	c2	$Pr_{0.9}K_{0.1}MnO_3$ [14]
17	c1	$Pr_{0.7}Ca_{0.3}MnO_3$ [17]	61	c1	$SrMnO_3$ [34]	104	c2	$Pr_{0.85}K_{0.15}MnO_3$ [45]
18	c1	$Pr_{0.6}Ca_{0.4}MnO_3$ [17]	62	c1	$Sr_{0.9}Ca_{0.1}MnO_3$ [34]	105	c2	$Pr_{0.8}Ba_{0.2}MnO_3$ [14]
19	c1	$Pr_{0.5}Ca_{0.5}MnO_3$ [18]	63	c1	$Sr_{0.8}Ca_{0.2}MnO_3$ [34]	106	c2	$Pr_{0.7}Sr_{0.3}MnO_3$ [46]
20	c1	$Pr_{0.5}Ca_{0.09}Sr_{0.41}MnO_3$ [18]	64	c1	$Sr_{0.7}Ca_{0.3}MnO_3$ [34]	107	c2	$Pr_{0.63}Sm_{0.07}Sr_{0.3}MnO_3$ [46]
21	c1	$Pr_{0.44}Sr_{0.56}MnO_3$ [19]	65	c1	$Sr_{0.6}Ca_{0.4}MnO_3$ [34]	108	c2	$Pr_{0.63}Bi_{0.07}Sr_{0.3}MnO_3$ [46]
22	c1	$Pr_{0.44}Sr_{0.56}MnO_3$ [19] (1.9 GPa)	66	c1	$Sr_{0.5}Ca_{0.5}MnO_3$ [34]	109	c2	$Pr_{0.5}Sr_{0.5}MnO_3$ [20]
			67	c1	$Sr_{0.4}Ca_{0.6}MnO_3$ [34]	110	c2	$Pr_{0.5}Sr_{0.5}MnO_3$ [19] (1.9 GPa)
23	c1	$Pr_{0.4}Ca_{0.6}MnO_3$ [17]	68	c1	$Sr_{0.3}Ca_{0.7}MnO_3$ [34]			
24	c1	$Pr_{0.4}Sr_{0.6}MnO_3$ [20]	69	c1	$Sr_{0.2}Ca_{0.8}MnO_3$ [34]	111	c2	$Pr_{0.5}S_{r0.46}Ca_{0.04}MnO_3$ [47]
25	c1	$Pr_{0.3}Ca_{0.7}MnO_3$ [17]	70	c1	$Sr_{0.1}Ca_{0.9}MnO_3$ [34]	112	c2	$Pr_{0.5}Sr_{0.45}Ba_{0.05}MnO_3$ [48]
26	c1	$Pr_{0.3}Sr_{0.7}MnO_3$ [20]	71	c1	$Sr_{0.9}Ba_{0.1}MnO_3$ [34]	113	c2	$Pr_{0.5}Sr_{0.41}Ca_{0.09}MnO_3$ [47]
27	c1	$Pr_{0.2}Ca_{0.8}MnO_3$ [17]	72	c1	$Sr_{0.8}Ba_{0.2}MnO_3$ [34]	114	c2	$Pr_{0.5}Sr_{0.38}Ca_{0.12}MnO_3$ [47]
28	c1	$Pr_{0.15}Sr_{0.85}MnO_3$ [21]	73	c1	$CaMnO_3$ [34]	115	c2	$Pr_{0.5}Sr_{0.3}Ca_{0.2}MnO_3$ [47]
29	c1	$Pr_{0.1}Ca_{0.9}MnO_3$ [17]	74	c1	$Ca_{0.975}Ce_{0.025}MnO_3$ [35]	116	c2	$Pr_{0.5}Sr_{0.3}Ba_{0.2}MnO_3$ [42]
30	c1	$Pr_{0.1}Sr_{0.9}MnO_3$ [22]	75	c1	$Ca_{0.95}Ce_{0.05}MnO_3$ [35]	117	c2	$Pr_{0.5}Sr_{0.2}Ba_{0.3}MnO_3$ [48]
31	c1	$NdMnO_3$ [23]	76	c1	$Ca_{0.925}Ce_{0.075}MnO_3$ [35]	118	c2	$Pr_{0.5}Sr_{0.1}Ba_{0.4}MnO_3$ [48]
32	c1	$Nd_{0.5}Ca_{0.5}MnO_3$ [11]	77	c2	$La_{0.9}Pr_{0.1}MnO_3$ [12]	119	c2	$Pr_{0.5}Ba_{0.5}MnO_3$ [48]
33	c1	$Nd_{0.45}Sr_{0.55}MnO_3$ [24]	78	c2	$La_{0.9}Ba_{0.1}MnO_3$ [36]	120	c2	$Pr_{0.46}Sr_{0.54}MnO_3$ [20]
34	c1	$Nd_{0.4}Sr_{0.6}MnO_3$ [24]	79	c2	$La_{0.86}Ba_{0.14}MnO_3$ [36]	121	c2	$Pr_{0.3}La_{0.2}Sr_{0.5}MnO_3$ [42]
35	c1	$Nd_{0.37}Sr_{0.63}MnO_3$ [24]	80	c2	$La_{0.85}Ca_{0.15}MnO_3$ [37]	122	c2	$Sm_{0.5}Sr_{0.5}MnO_3$ [11]
36	c1	$Nd_{0.3}Sr_{0.7}MnO_3$ [24]	81	c2	$La_{0.825}Ca_{0.175}MnO_3$ [37]	123	c2	$Sm_{0.6}Sr_{0.4}MnO_3$ [49]
37	c1	$Nd_{0.33}Sr_{0.67}MnO_3$ [24]	82	c2	$La_{0.8}Pr_{0.2}MnO_3$ [12]	124	c2	$Nd_{0.7}Ba_{0.3}MnO_3$ [50]
38	c1	$Nd_{0.25}Sr_{0.75}MnO_3$ [24]	83	c2	$La_{0.75}Ca_{0.25}MnO_3$ [38]	125	c2	$Nd_{0.7}Ba_{0.1}Sr_{0.2}MnO_3$ [50]
39	c1	$Sm_{0.5}Ca_{0.5}MnO_3$ [11]	84	c2	$La_{0.7}S_{r0.3}MnO_3$ [38]	126	c2	$Nd_{0.7}Ba_{0.2}Sr_{0.1}MnO_3$ [50]
40	c1	$Sm_{0.2}Ca_{0.8}MnO_3$ [25]	85	c2	$La_{0.7}Ba_{0.3}MnO_3$ [38]	127	c2	$Nd_{0.7}Ba_{0.25}Sr_{0.05}MnO_3$ [50]
41	c1	$Sm_{0.15}Ca_{0.85}MnO_3$ [21]	86	c2	$La_{0.55}Sr_{0.45}MnO_3$ [9]	128	c2	$Nd_{0.51}Sr_{0.49}MnO_3$ [24]
42	c1	$Sm_{0.1}Ca_{0.9}MnO_3$ [22]	87	c2	$La_{0.525}Pr_{0.175}Ca_{0.3}MnO_3$ [38]	129	c2	$Nd_{0.5}Sr_{0.5}MnO_3$ [11]
43	c1	$^{153}EuMnO_3$ [23]	88	c2	$La_{0.52}Y_{0.15}Ca_{0.33}MnO_3$ [39]	130	c2	$Nd_{0.49}Sr_{0.51}MnO_3$ [24]
44	c1	$TbMnO_3$ [26]	89	c2	$La_{0.5}Ca_{0.5}MnO_3$ [40]	131	c2	$Bi_{0.25}La_{0.25}Ca_{0.5}MnO_3$ [51]

observed-versus-*predicted plot* for each y variable (here T_N or T_C)—a so-called *coefficient diagram* from which the contribution (positive or negative) for the specific y variable is quantitatively seen.

Finally, PLS-DA [1] was performed to examine how the two compound classes, i.e. the AFM compounds (Class-1) and the FM compounds (Class-2), differ from each other, and to understand which CS/CC parameter(s) most strongly contribute in making the two classes of compounds different. In PLS-DA the X matrix consists of the same $21+1$ x variables as in PCA and PLS, whereas the class identity information is carried in the Y matrix which consists of so-called *dummy variables*, being just artificially generated combinations of ones and zeros (e.g. 1 0 for Class-1 compounds and 0 1 for Class-2 compounds). PLS is then performed to relate the two matrices, X and Y. As an outcome of PLS-DA, we obtain a coefficient diagram, which reveals the discriminatory power of each x variable.

The results of the aforementioned projection analyses are evaluated on the bases of two goodness-of-fit parameters: R^2 describes how much of the variation is explained by the model, while Q^2 describes the predictive power of the model. For a reasonable model Q^2 values larger than 0.5 are expected. Another criterion is that the R^2 and the

Q^2 values should not deviate too much. In the PLS analyses, R^2 is calculated separately for the X and Y matrices, i.e. R^2X and R^2Y.

3. Results and discussion

3.1. Class-1 (AFM $AMnO_3$ compounds)

Data analysis was started by performing PCA for the AFM compounds of Class-1 ($N_{AFM} = 76$). Calculation of three PCs resulted in a goodness-of-fit parameters of $R^2 = 0.903$ and $Q^2 = 0.861$. In Figs. 2(a) and (b) the obtained score and loading plots, respectively, are displayed. From Fig. 2(a) it is concluded that all the 76 samples are located either inside or in the very vicinity of the ellipse that defines the boundary of the 95% confidence region of the model; in other words, no outliers are detected in the data set. Also concluded is that the samples do not form obvious clusters inside the ellipse. At the same time, overall inspection of the loading plot of Fig. 2(b) reveals that all the 22 variables (i.e. the 21 CS/CC parameters *plus* the T_N value) included in the model are important as all of them are located relatively far from the origin of the plot. Further interpretation of the loading plot reveals that, for instance, the Mn–O–Mn bond angles [*alpha*, *beta* and $\langle$Mn–O–Mn$\rangle$] and the average A-site cation radius [$r(A)$] are situated close to each other and also close to the magnetic transition temperature (T_N), indicating that strong positive correlations exist among them. In other words, an increase in $r(A)$ results in a less-tilted MnO_6 octahedron network, which in turn should be beneficial for the super-exchange-mediated AFM interactions based on 180° cation–anion–cation interactions [54]. On the other hand, the structural distortion parameters, i.e. Jahn–Teller distortion (JT), MnO_6-octahedron distortion (*delta*), average apical compression (*epsilon*) and deviation of the tolerance factor from unity [$(1-TF)^2$], are all found farthest from T_N in Fig. 2(b). This means that these parameters correlate negatively with T_N, being in line with the principles of the super-exchange mechanism and the fact that the less efficient overlap of Mn and O orbitals weakens the AFM coupling. In other words, once the deformation of the MnO_6 octahedron diminishes such that

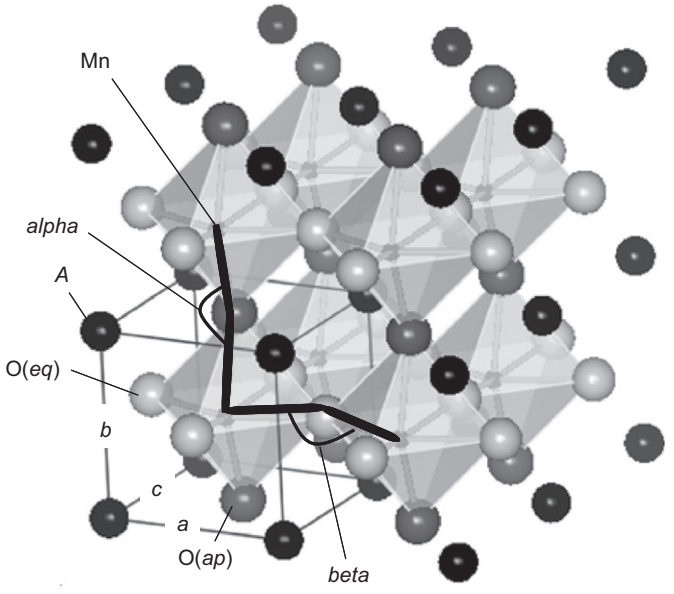

Fig. 1. Definitions of the crystal-structure parameters used in the present analyses.

Table 2
List of original variables and their explanations/definitions

Variable	Explanation	Definition
a, b, c	Lattice parameters *per* perovskite unit	
Vol	Volume *per* perovskite unit	$\mathrm{Vol} \equiv a \times b \times c$
$r(A)$	Average ionic radius at the A-site	
$V(A)$	Average valence of A cations	
Mn − O(*ap*) Mn − O(*eq*)*l* Mn − O(*eq*)*s*	Different Mn–O bond lengths (*l*: longer, *s*: shorter)	
$\langle$Mn–O$\rangle$	Average Mn–O bond length	
Alpha	Mn–O(*ap*)—Mn bond angle	
Beta	Mn–O(*eq*)—Mn bond angle	
$\langle$Mn–O–Mn$\rangle$	Average Mn–O–Mn bond angle	
TF	Tolerance factor	$\mathrm{TF} \equiv (r_A + r_O)/\sqrt{2}(r_{Mn} + r_O)$
(1−TF)2	Deviation of tolerance factor from unity	$(1-\mathrm{TF})2 \equiv (1-\mathrm{TF})^2$
Sigma2	A-site cationic size mismatch	$sigma2 \equiv \sigma^2 = \sum_i y_i r_i^2 - \langle r_A \rangle^2$
BVS(Mn)	Valence of Mn estimated from bond-valence-sum calculation	
JT	Jahn–Teller parameter	$\mathrm{JT} \equiv \sqrt{1/3\sum_i[(\mathrm{Mn}-\mathrm{O}_i) - \langle \mathrm{Mn}-\mathrm{O}\rangle]^2}$
Delta	MnO_6-octahedron distortion parameter	$delta \equiv \Delta = 1/N\sum_n[(\mathrm{Mn}-\mathrm{O})_n - \langle \mathrm{Mn}-\mathrm{O}\rangle/\langle \mathrm{Mn}-\mathrm{O}\rangle]^2$
Epsilon	Average apical compression	$epsilon \equiv \varepsilon = \lvert\langle \mathrm{Mn}-\mathrm{O(eq)}\rangle/\mathrm{Mn}-\mathrm{O(ap)} - 1\rvert$
W	Bandwidth-related parameter	$W \equiv \cos\omega/\langle \mathrm{Mn}-\mathrm{O}\rangle^{3.5}$, where $\omega = 1/2(\pi - \langle \mathrm{Mn}-\mathrm{O}-\mathrm{Mn}\rangle)$

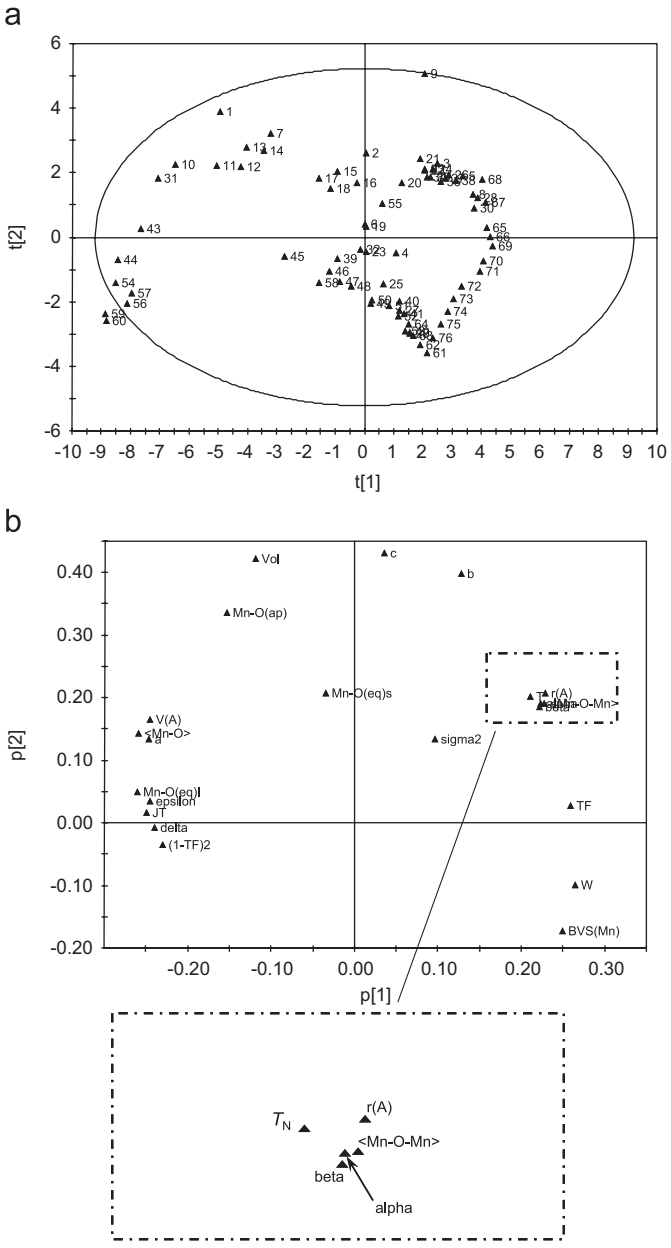

Fig. 2. PCA (a) score and (b) loading plots for the AFM $A\mathrm{MnO_3}$ compounds of Class-1.

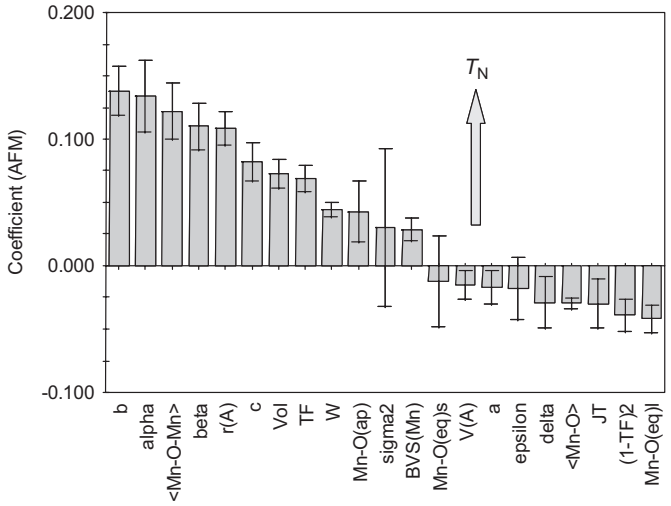

Fig. 3. Coefficient diagram for T_N in AFM $A\mathrm{MnO_3}$ compounds (Class-1). For each parameter the 95% confidence interval is indicated.

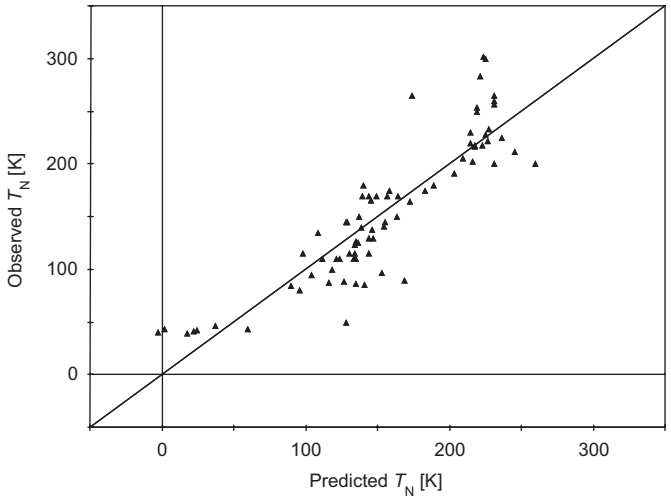

Fig. 4. Observed versus predicted plot for T_N in antiferromagnetic $A\mathrm{MnO_3}$ compounds (Class-1).

the crystal structure approaches the ideal perovskite structure strong AFM coupling with a high T_N value is realized, which is in a straightforward manner revealed from the present PCA results.

To model the relation between the CS/CC parameters and the value of T_N, PLS was performed by two PCs ($R^2X = 0.809$, $R^2Y = 0.786$ and $Q^2 = 0.771$). As in the case of PCA, no outliers were diagnosed as all the observations were found within the ellipse of 95% confidence (not shown here). The PLS coefficient diagram is given in Fig. 3. Such a diagram reveals the distinct impact (positive or negative) of each crystal-chemical parameter on T_N. As expected on the bases of PCA, the Mn–O–Mn bond angles (*alpha*, *beta* and $\langle$Mn–O–Mn$\rangle$) present strong positive influence on T_N, whereas the structural distortion parameters (JT, *delta*, *epsilon* and $(1-\mathrm{TF})^2$) exhibit negative (and somewhat weaker) impacts on T_N. Lattice parameter *b* is also shown to have a strong positive impact on T_N (see Fig. 3). We attribute this to the fact that bond lengths in general fluctuate less than the lattice parameters. Then with increasing *b*, *alpha* also increases as the position of O(*ap*) changes, i.e. there is a strong positive correlation between *b* and *alpha*. Hence, we may conclude that to design an $A\mathrm{MnO_3}$ perovskite with a high T_N value, we should aim at a less-tilted $\mathrm{MnO_6}$ octahedron. Finally, the observed-versus-predicted T_N is shown in Fig. 4. All the samples fall in a satisfactory manner on the diagonal, confirming that our model is valid. Hence, we conclude that for the AFM $A\mathrm{MnO_3}$ compounds we have been able to

satisfactorily model the relationships between CS/CC parameters and T_N by means of the employed multivariate data analysis techniques.

3.2. Class-2 (FM $AMnO_3$ compounds)

We performed PCA for the Class-2 FM compounds ($N_{FM} = 55$) in a way parallel to that for the AFM compounds of Class-1. The results are shown in Figs. 5(a) and (b). PCA with four PCs ended up with the goodness-of-fit parameters of $R^2 = 0.873$ and $Q^2 = 0.712$. The various relationships among the magnetic transition temperature (T_C) and the CS/CC parameters resemble those seen for the Class-1 compounds. Especially, in the loading plot for Class-2 (Fig. 5(b)), the various parameters are found roughly about the same positions as in the case of Class-1 compounds, reflecting the fact that a less-tilted MnO_6 network also results in a higher T_C among the FM $AMnO_3$ compounds. However, for Class-2 no clear grouping among the variables is seen (at least to the same extend as for Class-1), indicating that correlation between the T_C value and the CS/CC parameters is rather weak. This is in accordance with our empirical knowledge that the crystal structure becomes more symmetric because of the weakening or disappearance of the Jahn–Teller effect when ferromagnetism is induced through doping (i.e. divalent-for-trivalent A-site cation substitution) in the parent AFM Jahn–Teller-active $AMnO_3$ lattice. In Fig. 6, individual R^2 and Q^2 values are shown for each of the 22 variables used in the PCA modeling, both for the Class-1 and the Class-2 compounds. For Class-1, most of the variables are well described by the PCA model (Fig. 6 (a)), whereas for Class-2 large differences between the R^2 and Q^2 values are seen for some of the variables (e.g. *sigma*2, *a*, *b*, *c*, Mn–O(*ap*), Mn–O(*eq*)*s*, *T*, *epsilon*) (Fig. 6 (b)). These variables, except for *sigma*2 and T_C, are related to the shape of the MnO_6 octahedron.

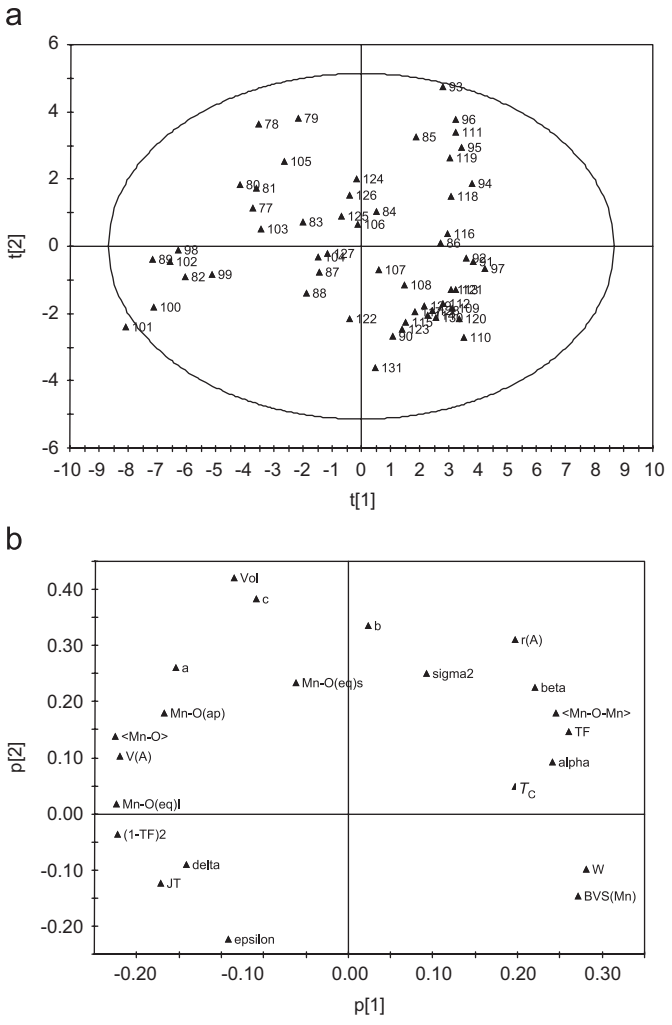

Fig. 5. PCA (a) score and (b) loading plots for the FM $AMnO_3$ compounds of Class-2.

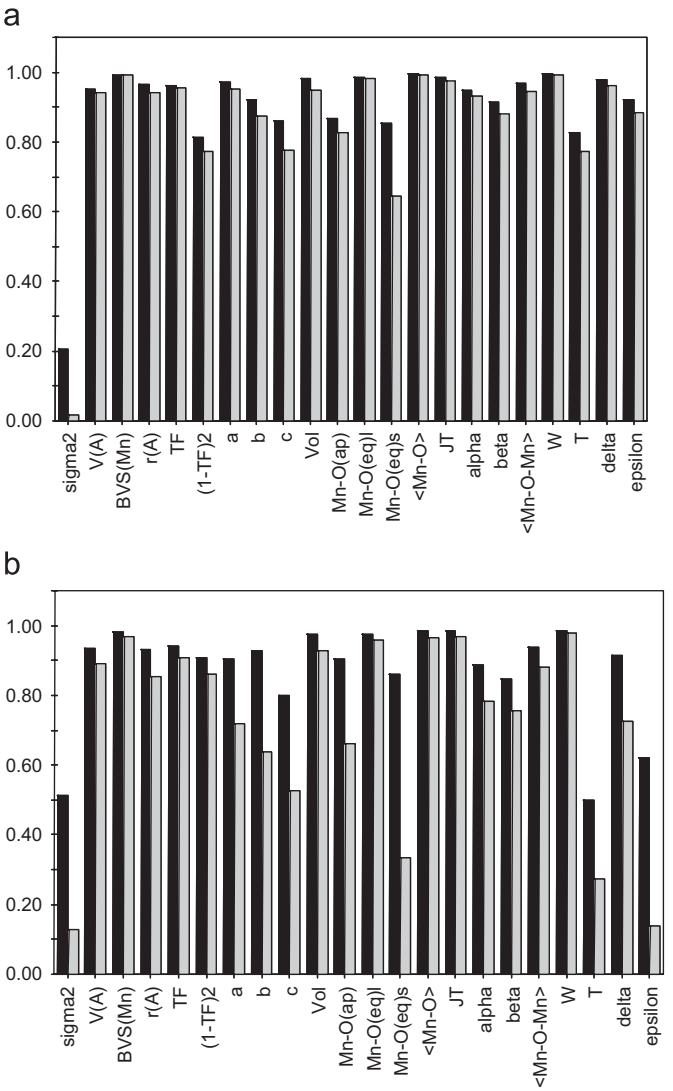

Fig. 6. Individual R^2 and Q^2 values for all the 22 variables after PCA for (a) Class-1 and (b) Class-2. Left black bar and right gray bar represent the R^2 and Q^2 values, respectively.

Somewhat similar difficulties were encountered when the PLS analysis was attempted for Class-2. It was not possible to model the structure–property relationships in a satisfactory manner: the obtained Q^2 value was smaller than 0.5, which has been regarded as the lowest limit for good prediction power in PLS. The result is a supporting argument for the weak structure–property relations in FM $A\mathrm{MnO_3}$ compounds. However, we should also consider the raw data set. Ferromagnetism among the perovskite manganese oxides is rather rare, appearing only in a narrow composition area. Hence our data set for Class-2 consists of 55 samples that are very similar to each other in terms of CS/CC parameters. For such a system, multivariate data analysis may not work efficiently/properly.

3.3. Discrimination between FM and AFM $A\mathrm{MnO_3}$ compounds

Even though it was not possible to properly model the T_C on the bases of CS/CC parameters for the FM manganese-oxide perovskites, we wanted to see how different the FM $A\mathrm{MnO_3}$ compounds are from the AFM $A\mathrm{MnO_3}$ compounds and to find (if possible) some clues for the most influential/characteristic CS/CC parameters that differentiate the two classes of compounds from each other. Hence the class discriminating characteristics were searched for by means of PLS-DA carried out for the entire data set of all the 131 samples ($N_{\mathrm{TOT}} = 131$) with the 21 CS/CC parameters as x variables. Calculation of three PCs yielded the goodness-of-fit parameters as: $R^2X = 0.891$, $R^2Y = 0.526$ and $Q^2 = 0.507$. Fig. 7(a) displays the score plot to demonstrate that the two classes are clearly separated from each other. Quantitative measures for the discriminatory power of each individual x variable are seen from the PLS-DA coefficient diagram presented in Fig. 7(b). From Fig. 7(b) revealed is that the parameters, *c*, Mn–O(*eq*)*s* and Mn–O(*ap*) (i.e. decreased distortion of $\mathrm{MnO_6}$ octahedron), have the strongest positive contribution to the identity of Class-2 FM compounds, while *epsilon*, JT, TF and *delta* (i.e. increased distortion of $\mathrm{MnO_6}$ octahedron) contribute most strongly to the identity of Class-1 AFM compounds. This agrees with our empirical belief that the Class-2 FM compounds are more isotropic than the Class-1 AFM compounds (regarding the $\mathrm{MnO_6}$ octahedron). Also seen in Fig. 7(b) is that both *sigma*2 and $V(A)$ have a positive impact on the appearance of FM in manganese-oxide perovskites. This is natural since FM emerges in the $A\mathrm{MnO_3}$ system only (in a narrow compositional range) when the $A\mathrm{MnO_3}$ phase is doped to contain mixed-valent $\mathrm{Mn^{III/IV}}$ through partial divalent-for-trivalent cation substitution at the A site, whereas AFM is found both in the non-doped $A^{\mathrm{III}}\mathrm{Mn^{III}O_3}/A^{\mathrm{II}}\mathrm{Mn^{IV}O_3}$ and doped $\mathrm{A^{II/III}Mn^{III/IV}O_3}$ compounds. Hence the critical point for stabilizing the rare FM state in the $A\mathrm{MnO_3}$ system is how we would be able to diminish the distortion of the $\mathrm{MnO_6}$ octahedron in the required range of doping,

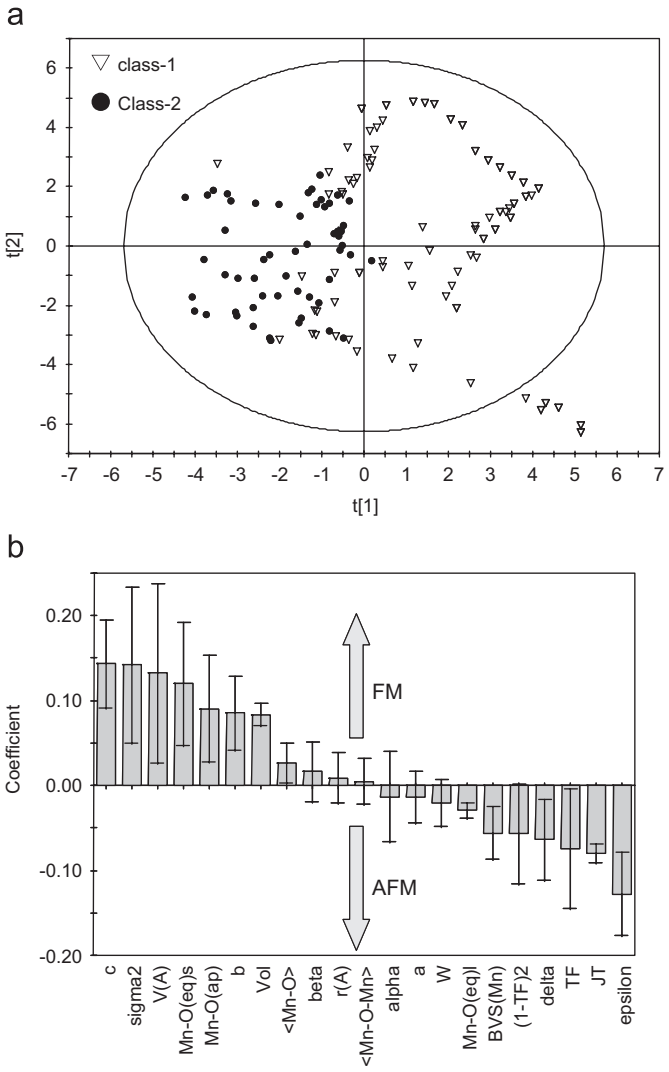

Fig. 7. PLS-DA for 131 samples of (AFM or FM) $A\mathrm{MnO_3}$ compounds: (a) scores plot revealing a nearly perfect separation of the data into the two groups of AFM (Class-1) and FM (Class-2) compounds and (b) coefficients diagram to show the importance of the 21 x variables used in the analysis to discriminate the FM $A\mathrm{MnO_3}$ compounds (Class-2) from those of AFM $A\mathrm{MnO_3}$ compounds (Class-1).

i.e. at the proper $V(A)$ value. One of the tickets for this as proposed by the present analysis is to elongate the crystal along z-axis to elongate *c* and Mn–O(*eq*)*s* [or to elongate *b* and Mn–O(*ap*)], but not to increase *epsilon* (Fig. 7(b)).

4. Conclusion

The present pioneering work has demonstrated that multivariate data analysis techniques (PCA, PLS and PLS-DA) are potentially useful for understanding the structure–property relationships in perovskite manganese oxides. The target group of compounds consisted of 131 samples of oxygen-stoichiometric $A\mathrm{MnO_3}$ perovskites (either AFM or FM) with different A-site cation compositions. For the AFM compounds, the structure–property relations were successfully modeled so as to be able to

predict the value of T_N on the bases of crystal-structure/crystal-chemical parameters only and to elucidate contributions of the individual parameters. In contrast, for the FM compounds parallel treatment did not produce usable results presumably due to weaker structure-property relations (compared to the AFM compounds) and/or the narrowness of the FM region (in terms of chemical composition) in the magnetic phase diagram of the $A\mathrm{MnO_3}$ system. On the other hand, discrimination analysis was successfully employed to demonstrate that the FM $A\mathrm{MnO_3}$ compounds are clearly different from the AFM $A\mathrm{MnO_3}$ compounds in their crystal-structure/crystal-chemistry fine-features. As revealed from the present multivariate analysis, the most important prerequisite for the FM state to appear in the $A\mathrm{MnO_3}$ system is that (besides creating the proper mixed-valence state for Mn) one should be able to shape the $\mathrm{MnO_6}$ octahedron isotropic enough.

Acknowledgment

This work was supported by Academy of Finland (Decision Nos. 114517 and 116254).

References

[1] L. Eriksson, E. Johansson, N. Kettaneh-Wold, S. Wold, Multi- and Megavariate Data Analysis: Principles and Applications, Umetrics, Umeå, Sweden, 2001.
[2] K. Lehmus, M. Karppinen, J. Solid State Chem. 162 (2001) 1.
[3] A.R. Katritzky, D.C. Fara, M. Kuanar, E. Hur, M. Karelson, J. Phys. Chem. A 109 (2005) 10323.
[4] C. Suh, K. Rajan, QSAR Combinat. Sci. 24 (2005) 114.
[5] S. Gadzuric, C. Suh, M. Gaune-Escard, K. Rajan, Metall. Mater. Trans. A 37 (2006) 3411.
[6] J.R. Nowers, S.R. Broderick, K. Rajan, B. Narasimhan, Macromol. Rapid Commun. 28 (2007) 972.
[7] J. Rodríguez-Carvajal, M. Hennion, F. Moussa, A.H. Moudden, L. Pinsard, A. Revcolevschi, Phys. Rev. B 57 (1998) R3189.
[8] P. Dai, J. Zhang, H.A. Mook, S.-H. Liou, P.A. Dowben, E.W. Plummer, Phys. Rev. B 54 (1996) R3694.
[9] O. Chmaissem, B. Dabrowski, S. Kolesnik, J. Mais, J.D. Jorgensen, S. Short, Phys. Rev. B 67 (2003) 094431.
[10] M.T. Fernández-Díaz, J.L. Martínez, J.M. Alonso, E. Herrero, Phys. Rev. B 59 (1999) 1277.
[11] P.M. Woodward, T. Vogt, D.E. Cox, A. Arulraj, C.N.R. Rao, P. Karen, A.K. Cheetham, Chem. Mater. 10 (1998) 3652.
[12] V. Dyakonov, F. Bukhanko, V. Kamenev, E. Zubov, S. Baran, T. Jaworska-Gołąb, A. Szytuła, E. Wawrzyńska, B. Penc, R. Duraj, N. Stűsser, M. Arciszewska, W. Dobrowolski, K. Dyakonov, J. Pientosa, O. Manus, A. Nabialek, P. Aleshkevych, R. Puzniak, A. Wisniewski, R. Zuberek, H. Szymczak, Phys. Rev. B 74 (2006) 024418.
[13] D. Sánchez, J.A. Alonso, M.J. Martínez-Lope, J. Chem. Soc. Dalton Trans. (2002) 4422.
[14] Z. Jirák, J. Hejtmánek, E. Pollert, M. Maryško, M. Dlouhá, S. Vratislav, J. Appl. Phys. 81 (1997) 5790.
[15] D.P. Kozlenko, V.P. Glazkov, Z. Jirák, B.N. Savenko, J. Magn. Magn. Mater. 267 (2003) 120.
[16] D.P. Kozlenko, Z. Jirák, I.N. Goncharenko, B.N. Savenko, J. Phys.: Condens. Matter 16 (2004) 5883.
[17] Z. Jirák, S. Krupička, Z. Šimša, M. Dlouhá, S. Vratislav, J. Magn. Magn. Mater. 53 (1985) 153.
[18] Z. Jirák, F. Damay, M. Hervieu, C. Martin, B. Raveau, G. André, F. Bourée, Phys. Rev. B 61 (2000) 1181.
[19] D.P. Kozlenko, V.P. Glazkov, Z. Jirák, B.N. Savenko, J. Phys.: Condens. Matter 16 (2004) 2381.
[20] K. Knížek, J. Hejtmánek, Z. Jirák, C. Martin, M. Hervieu, B. Raveau, G. André, F. Bourée, Chem. Mater. 16 (2004) 1104.
[21] C. Martin, A. Maignan, M. Hervieu, B. Raveau, Z. Jirák, A. Kurbakov, V. Trounov, G. André, F. Bourée, J. Magn. Magn. Mater. 205 (1999) 184.
[22] C. Martin, A. Maignan, M. Hervieu, B. Raveau, Z. Jirák, M.M. Savosta, A. Kurbakov, V. Trounov, G. André, F. Bourée, Phys. Rev. B 62 (2000) 6442.
[23] B. Dabrowski, S. Kolesnik, A. Baszczuk, O. Chmaissem, T. Maxwell, J. Mais, J. Solid State Chem. 178 (2005) 629.
[24] R. Kajimoto, H. Yoshizawa, H. Kawano, H. Kuwahara, Y. Tokura, K. Ohoyama, M. Ohashi, Phys. Rev. B 60 (1999) 9506.
[25] C. Autret, C. Martin, A. Maignan, M. Hervieu, B. Raveau, G. André, F. Bourée, A. Kurbakov, V. Trounov, J. Magn. Magn. Mater. 241 (2002) 303.
[26] J. Blasco, C. Ritter, J. García, J.M. de Teresa, J. Pérez-Cacho, M.R. Ibarra, Phys. Rev. B 62 (2000) 5609.
[27] A. Mahcida, Y. Moritomo, K. Ohoyama, A. Nakamura, J. Phys. Soc. Jpn. 70 (2001) 3739.
[28] A. Muñoz, M.T. Casáis, J.A. Alonso, M.J. Martínez-Lope, J.L. Martínez, M.T. Fernández-Díaz, Inorg. Chem. 40 (2001) 1020.
[29] C. Autret, C. Martin, A. Maignan, M. Hervieu, B. Raveau, G. André, F. Bourée, J. Solid State Chem. 165 (2002) 65.
[30] J.A. Alonso, M.J. Martínez-Lope, M.T. Casais, M.T. Fernández-Díaz, Inorg. Chem. 39 (2000) 917.
[31] Y.H. Huang, H. Fjellvåg, M. Karppinen, B.C. Hauback, H. Yamauchi, J.B. Goodenough, Chem. Mater. 18 (2006) 2130.
[32] H. Okamoto, N. Imamura, B.C. Hauback, M. Karppinen, H. Yamauchi, H. Fjellvåg, Solid State Commun. 2008, in press.
[33] M. Dlouhá, S. Vratislav, Z. Jirák, J. Hejtmánek, K. Knížek, D. Sedmidubský, Appl. Phys. A 74 (2002) S673.
[34] O. Chmaissem, B. Dabrowski, S. Kolesnik, J. Mais, D.E. Brown, R. Kruk, P. Prior, P. Pyles, J.D. Jorgensen, Phys. Rev. B 64 (2001) 134412.
[35] E.N. Caspi, M. Avdeev, S. Short, J.D. Jorgensen, M.V. Lobanov, Z. Zeng, M. Greenblatt, P. Thiyagarajan, C.E. Botez, P.W. Stephens, Phys. Rev. B 69 (2004) 104402.
[36] B. Dabrowski, K. Rogacki, X. Xiong, P.W. Klamut, R. Dybzinski, J. Shaffer, J.D. Jorgensen, Phys. Rev. B 58 (1998) 2716.
[37] M. Pissas, I. Margiolaki, G. Papavassiliou, D. Stamopoulos, D. Argyriou, Phys. Rev. B 72 (2005) 064425.
[38] P.G. Radaelli, G. Iannone, M. Marezio, H.Y. Hwang, S-W. Cheong, J.D. Jorgensen, D.N. Argyriou, Phys. Rev. B 56 (1997) 8265.
[39] J.L. García-Muñoz, M. Suaaidi, J. Fontcuberta, J. Rodríguez-Carvajal, Phys. Rev. B 55 (1997) 34.
[40] P.G. Radaelli, D.E. Cox, M. Marezio, S-W. Cheong, Phys. Rev. B 55 (1997) 3015.
[41] J. Spooren, R.I. Walton, F. Millange, J. Mater. Chem. 15 (2005) 1542.
[42] C. Autret, C. Martin, M. Hervieu, A. Maignan, B. Raveau, G. André, F. Bourée, Z. Jirak, J. Magn. Magn. Mater. 270 (2004) 194.
[43] O. Chmaissem, B. Dabrowski, S. Kolesnik, J. Mais, L. Suescun, J.D. Jorgensen, Phys. Rev. B 74 (2006) 144415.
[44] S. Megdiche, M. Ellouze, A. Cheikh-Rouhou, Q. Cai, W.B. Yelon, J. Alloys Compd. 348 (2003) 30.
[45] Z. Jirák, J. Hejtmánek, K. Knížek, R. Sonntag, J. Solid State Chem. 132 (1997) 98.
[46] M. Ellouze, Q. Cai, W.B. Yelon, J. Alloys Compd. 386 (2005) 20.
[47] F. Damay, C. Martin, A. Maignan, M. Hervieu, B. Raveau, Z. Jirak, G. André, F. Bourée, Chem. Mater. 11 (1999) 536.
[48] C. Autret, C. Martin, M. Hervieu, A. Maignan, B. Raveau, G. André, F. Bourée, Z. Jirak, Chem. Mater. 15 (2003) 1886.
[49] I.D. Luzyanin, V.A. Ryzhov, D.Yu. Chernyshov, A.I. Kurbakov, V.A. Trounov, A.V. Lazuta, V.P. Khavronin, I. Larionov, S.M. Dunaevsky, Phys. Rev. B 64 (2001) 094432.

[50] E. Suard, F. Fauth, C. Martin, A. Maignan, F. Millange, L. Keller, J. Magn. Magn. Mater. 264 (2003) 221.
[51] K.A. Krezhov, D. Kovacheva, E. Sváb, F. Bourée, J. Phys.: Condens. Matter 17 (2005) S3139.
[52] R.D. Shannon, Acta Crystallogr. Sect. A 32 (1976) 751.
[53] Y.Q. Jia, J. Solid State Chem. 95 (1991) 184.
[54] See for example, J.B. Goodenough, Magnetism and the Chemical Bond, Krieger, Huntington, 1976.